

---

## Multiscale analysis of living benthic foraminiferal heterogeneity: Ecological advances from an intertidal mudflat (Loire estuary, France)

Thibault de Chanvalon A. <sup>1,\*</sup>, Geslin E. <sup>2</sup>, Mojtahid M. <sup>2</sup>, Métais I. <sup>3</sup>, Méléder V. <sup>4</sup>, Metzger E. <sup>2</sup>

<sup>1</sup> CNRS, Université de Pau et des Pays de l'Adour, E2S UPPA, IPREM, Pau, France

<sup>2</sup> Univ Angers, Université de Nantes, CNRS, LPG, F-49000 Angers, France

<sup>3</sup> Université Catholique de l'Ouest, BIOSSE, Angers, France

<sup>4</sup> Nantes Université, Institut des Substances et Organismes de la Mer, ISOMer, UR 2160, Nantes, France

\* Corresponding author : A. Thibault de Chanvalon, email address :

[aubin.thibault-de-chanvalon@univ-pau.fr](mailto:aubin.thibault-de-chanvalon@univ-pau.fr)

---

### Abstract :

An unprecedented sampling effort on the Loire estuary allowed a multi scale approach to identify parameters controlling density variations of benthic foraminifera. Indeed, the distances between the samples analysed for this study vary from 1 cm to hundreds of kilometres. To catch this range of distance variations, a model called Scale Variance Analysis was build describing the participation of each scale to the total observed variance. The SVA model requires, for each scale, the stability of relative variance. A comparison with the Moran's Index and experimental variogram is proposed showing coherent conclusions with the SVA analysis. The analysis shows that in order to maximize information on foraminiferal density variation, sampling campaigns should be designed with stations distant from few meters to 1 km, with a particular focus on the hectometre scale. A range of scale too rarely investigated in the community of benthic foraminifera ecology. Next, based on two intertidal mudflat stations separated of few hundred meters, the present study shows that for *Ammonia tepida*, the scale dependant preponderant parameters is the Chl a concentration in the top first centimetre. Contrastingly, the indicators of food quality such as the lability index and the oxygen penetration depth do not seem to affect *A. tepida* densities. This high quantity, low quality diet is interpreted as an opportunistic behaviour that is indirectly confirmed by a kinetic approach. This approach compares the deep infaunal microhabitat density with the shallow infaunal microhabitat density. The identical ratio indicates quick saturation of the available resources.

---

## Highlights

► A new indicator to quantify spatial heterogeneity among different scale, the Scale Variance Analysis (SVA), is proposed. ► It reveals higher heterogeneity of *Ammonia tepida* between 1 and 1000 m, in agreement with Moran's Index and experimental variogram. ► At the hectometer scale, direct correlation of *A. tepida* density with Chl a is observed. ► Equilibrium between deep and shallow infaunal population is rapidly reached for *A. tepida* probably due to rapid saturation of environmental capabilities.

## 2 Introduction

41

42

43 Benthic foraminifera are ubiquitous in sediment, giving them the potential to be bio-  
44 indicators of ecosystem functioning in all marine environments including transitional areas  
45 such as intertidal mudflats (e.g. Debenay et al., 2001; Schönfeld et al., 2012). Moreover, their  
46 distribution evolves monthly to seasonally (Alve and Murray, 2001; Kitazato et al., 2000)  
47 which fits with the frequency of most survey sampling and smooths the influence of  
48 environmental parameters that changes more rapidly (*e. g.* semi-diurnal tides). However, a  
49 comprehensive framework of their spatial heterogeneity is still lacking, while it could be an  
50 important step towards a standardization of the sampling strategy required for the  
51 optimization and generalization of their use as bio-indicators (Schönfeld et al., 2012).  
52 Additionally, assuming that a consequence has similar heterogeneity that its cause, multiscale  
53 analysis of heterogeneity would improve our understanding of the preponderant parameters  
54 controlling species distribution (*e. g.* Talley 2007).

55 Since the 50's, ecological studies take advantage of some mining engineer geostatistical  
56 methods to express the spatial distribution variability using synthetic indices (Legendre and  
57 Fortin, 1989). For example, the Moran's Index (Moran, 1950) has been applied on benthic  
58 foraminifera by Hohenegger et al. (1993) and Thibault de Chanvalon et al. (2015) to identify  
59 scales of patchiness. However, in the case of our study from the Loire estuary, to compare  
60 samples acquired at different spatial resolutions, and with a different sampling size, scale  
61 variance analysis is better-suited (Moellering and Tobler, 1972). In the Loire estuary,  
62 Mojtahid et al. (2016) documented the spatial distribution patterns of living foraminifera at a  
63 kilometric to decametric scale using a Van Veen grab sampler while Thibault de Chanvalon et  
64 al. (2015) described foraminiferal distribution based on 1 cm<sup>3</sup> samples from the intertidal

65 mudflat “Les Brillantes”. New data from 6 sites on the “Les Brillantes” mudflat distant from  
66 few metres to hundreds of metre are here gathered with the Mojtahid et al. (2016) and the  
67 Thibault de Chanvalon et al. (2015) datasets.

68 In the present paper, we will illustrate the role of such geostatistical tools to characterise the  
69 preponderant factor controlling some species distribution following a three steps demarche  
70 consisting in i) exploring, ii) identifying and iii) validating the causality relationship. In the  
71 case of the *Ammonia tepida* density distribution in the Loire estuary, we will i) determine the  
72 most significant scale to assess spatial foraminiferal density variation based on multiscale  
73 analyses, in order to ii) identify the preponderant mechanism controlling foraminifera density  
74 assuming it has a similar heterogeneity. This second step will be achieved looking at direct  
75 correlation with foraminifera density. To validate this deterministic approach we will iii) test  
76 the steady state between foraminifera density and the controlling factor based on vertical  
77 distribution analysis. Hence, with depth, different microhabitat characterised by different  
78 feeding time, exchange their population due to mobility or bioturbation. We will demonstrate  
79 that equilibrium between the density of these microhabitats indicate steady state regime at all  
80 depths.

81

## 3 Materials and methods

### 3.1 Study area

“Les Brillantes” mudflat is located in the inner part of the Loire River estuary (Figure 1), the outlet of a 117,045 km<sup>2</sup> - drainage basin composed of both sedimentary and granitic rocks. The mean discharge of the Loire River is 900 m<sup>3</sup>s<sup>-1</sup>, varying from 120 m<sup>3</sup>s<sup>-1</sup> in summer to over 5000 m<sup>3</sup>s<sup>-1</sup> during winter flood, and leading to a high seasonal variability of water salinity at “Les Brillantes”. The Loire estuary is macrotidal and hyper-synchronous (Le Floch, 1961) with a tidal range from 2 to 7 m, producing large intertidal areas (“Les Brillantes” is 1350 ha) and important sediment resuspension. Therefore, sediment grain size characteristics at “Les Brillantes” is quite homogeneous with silty-clay unimodal deposits with a median size of between 10 and 20 μm (Coynel et al., 2016). The 12 hours tidal cycling produces large daily changes of salinity and structuration of water column, especially when it chimes with low flow (that mostly varies seasonally, see Thibault de Chanvalon et al., 2016) and high tidal intensity (whose main cycle lasts 2 weeks). Depending on the period of the year, the moment of the lunar cycle and the time of the tidal cycle, salinity at the sampling point can vary from 35 to 0 and was about 20 in May 2013 and 14 in September 2012.

Two stations on the unvegetated slikke were chosen to study the spatial variability at the metre scale in “Les Brillantes” mudflat (Figure 1): Site 1 is located 20 m offshore from a 1 m-high-eroded cliff while Site 2 is 500 m offshore. The main difference between the two stations lies in the longer emersion time for site 1, the closest to the shore. According to Benyoucef (2014), Site 1 is characterized by a denser biofilm (*i.e.* microphytobenthos composed of diatoms).

### 3.2 Sampling strategies

106 In this study, the estimation of metric heterogeneity for micro and meiofaunal (*i.e.*  
107 foraminifera) composition is based on three replicate interface cores (triplicates cores) from  
108 the same site, distant from each other by few meters. For all the other measured parameters  
109 (oxygen profiles, macrofauna), a dedicated core was sampled from each site. A similar  
110 vertical sampling resolution was used for all analyses *i. e.* cores with inner diameter of 8.2  
111 cm, were sliced every 2 mm until 2 cm and every 5 mm until 5 cm with the exception of  
112 macrofauna of which the abundance was determined for the full core depth. To minimise the  
113 temporal variability, the foraminifera samples were acquired in September 2012 and May  
114 2013, simultaneously to those from Mojtahid et al. (2016, sampled in September 2012) and  
115 Thibault de Chanvalon et al., 2016.

### 116 **3.3 Biological compartment**

117 The core triplicate dedicated to foraminifera was sliced few hours after recovery and  
118 incubated overnight in Cell-Tracker™ Green (Invitrogen Detection Technologies) /  
119 dimethylsulfoxide (DMSO) mixture (final concentration of 1  $\mu\text{mol L}^{-1}$ ) then preserved in 10%  
120 formaldehyde / 3.8% borate mixture. This method was chosen for its accuracy at  
121 discriminating living from dead foraminifera since it reacts with enzymes to produce a  
122 fluorescent compound (see details in Bernhard et al., 2006). Only the larger (>150  $\mu\text{m}$ )  
123 fraction including adult specimens was conserved for identification (see detailed procedure in  
124 Langlet et al., 2014). Then, only foraminifera fluorescing continuously and brightly under an  
125 epifluorescent binocular (Olympus SZX12 with a fluorescent light source Olympus URFL-T)  
126 were picked out, counted and determined. Note that, the species that we refer to as *Ammonia*  
127 *tepida* in the following text corresponds to the phylotype T6 according to the recent  
128 classification of *Ammonia* sp. (Richirt et al., 2019). This is a common *Ammonia* phylotype in  
129 the European intertidal mudflats (Bird et al., 2020).

130 Foraminiferal oxygen uptake (FOU) is calculated with the equation (1), with  $R_i(T_{13})$  being  
131 the respiration rate of the species  $i$  from laboratory measurement at 13 °C in  $\text{pmol O}_2 \text{ ind}^{-1} \text{ d}^{-1}$   
132 from Geslin et al., 2011, the exponential being the Arrhenius temperature correction (with  $T_A$   
133 a constant in °C determined by Bradshaw, 1961) and  $d_i^0$  the measured areal density of living  
134 foraminifera in the oxic layer in  $\text{ind m}^{-2}$ :

$$\text{FOU} = \sum_i R_i(T_{13}) \exp\left(\frac{T_A}{T_{13}} - \frac{T_A}{T_{\text{obs}}}\right) d_i^0 \quad (1)$$

135

136 We calculated the average living depth  $ALD_x$ , initially proposed by Jorissen et al. (1995) to  
137 describe quantitatively the microhabitats distribution, following equation (2) :

$$ALD_x = \frac{\sum_i n_i D_i}{\sum_i n_i} \quad (2)$$

138 With  $n_i$  the number of specimens in interval  $i$ ,  $D_i$  the midpoint of sample interval and  $x$  the  
139 lower boundary of the deepest sample.

140 Another core triplicate was dedicated to microphytobenthos (MPB) and frozen *in situ* by  
141 liquid nitrogen. Pigments extraction used a cold mixture (4°C) of 90% methanol/0.2M  
142 ammonium acetate and 10% ethyl acetate (90/10 vol/vol) and measurement performed by  
143 HPLC (see Méléder et al., 2005 for details). To assess organic matter quality, we used the  
144 lability index,  $LI = \text{Chl } a / (\text{Chl } a + \text{Pheo } a)$ , with *Pheo a* corresponding to the total amount of  
145 phaeophorbides *a* and pheophytins *a*, respectively due to grazing and microbial activity (*e.g.*  
146 Bianchi and Findlay, 1991; Cartaxana et al., 2003).

147 Finally, each core of the triplicate dedicated to the macro-invertebrates was homogenized  
148 over its full depth (35cm) sieved at 1 mm and preserved in 4% formaldehyde before species  
149 identification and counting in the >1 mm fraction.

## 150 3.4 Oxygen fluxes

151 Dissolved oxygen vertical profiles were measured in a separate core in the dark, within few  
152 hours after sampling using a Clark-type microelectrode with a 50 µm thick tip (OX50,  
153 Unisense, Denmark) connected to a multimeter (Unisense) in a temperature controlled bath.  
154 Twelve and 10 oxygen profiles were measured in September 2012 and 24 and 4 profiles in  
155 May 2013 at stations S1 and S2 respectively. Diffusive O<sub>2</sub> uptake (DOU) was estimated with  
156 the PROFILE software by fitting the measured oxygen concentration with concentration from  
157 diffusion-reaction models (see details in Berg et al., 1998).

## 158 3.5 Statistical analysis

### 159 3.5.1 Moran's Index

160 Patchiness effect was explored using spatial correlograms built using the Moran's Index (I),  
161 computed with R (package "spdep" following Bivand and Wong, 2018 and Fortin and Dale,  
162 2005, Equation (3)). This index calculates the similarity of pair values for one neighbourhood  
163 compared to the global mean of the dataset, a neighbourhood being defined by a weighted  
164 ( $w_d$ ) function of the distance ( $l_{ij}$ ) between the pair values ( $x_i, x_j$ ). Here, we used a weighted  
165 function sensitive only to the scale of the distance, *i. e.*:

$$I(d) = \frac{\sum_i^n \sum_{j \neq i}^n w_d(l_{ij})(x_i - \bar{x})(x_j - \bar{x})}{\sum_i^n (x_i - \bar{x})^2} \times \frac{n_d}{\sum_{i,j}^n w_d(l_{ij})} \quad (3)$$

$$w_d(l_{ij}) = \begin{cases} 1, & 10^d < l_{ij} < 10^{d+1} \\ 0, & \text{otherwise} \end{cases} \quad (4)$$

166 and  $d$ , the scale of interest,  $n$ , the number of samples and  $n_d$  the number of samples forming  
167 at least one pair. Significance of values is estimated based on Monte-Carlo analyses provided  
168 in the "spdep" package (function `moran.mc`, done with 9999 simulations). This function  
169 compares the  $I$  value obtained from the original dataset with a distribution produced by many



170 simulated I values. First, these simulated I values were obtained by random distribution of all  
171 density values. Second, to take into account that in some case, very few sample formed pairs,  
172 the simulated I values were obtained by exchanging randomly 10% of the samples forming  
173 pairs with random samples from the dataset.

### 174 3.5.2 Scale Variance Analysis

175 Scale variance analysis (SVA) decomposes the total variance of a dataset to identify the  
176 contribution of each scale to the variance (Moellering and Tobler, 1972; Wu et al., 2000). The  
177 SVA compares each sample to a local mean which complements the Moran's Index, in which  
178 samples are compared to the global mean. This approach requires *a priori* explicit definition  
179 of scales of interest and *a priori* delimitation of all regions, necessarily nested over the  
180 different scales. By convention, for a dataset hierarchized over k scales of interest, the scale 1  
181 is the size of the initial samples, that are gathered in local regions belonging to the scale 2.  
182 Then, the mean of each local regions is treated as sample of the scale 2 and are gathered again  
183 in intermediate regions belonging to the scale 3. The process is repeated until the scale k,  
184 covering the extent over which the sampling has been done. On each scale, the concept of  
185 "scale variances" is introduced which corresponds to the variance of samples of scale h over a  
186 region of scale h+1.

187 The following details are inspired from Moellering and Tobler (1972) but using different  
188 writing. For samples of the scale h, gathered in regions belonging to the scale h+1, the scale  
189 variance,  $V_i^{h \rightarrow h+1}$ , is defined according to the equation (5).

$$V_i^{h \rightarrow h+1} = \frac{1}{n^h} \sum_{j=1}^{n^h} (x_i^{h+1} - x_{i,j}^h)^2 \quad (5)$$

190 With  $x_i^{h+1}$ , the mean value of all samples nested in the group i;  $x_{i,j}^h$  the different sample  
191 (whose size is belonging to the scale h) value constituting the group i and  $n^h$  the number of

192 sample  $x_{i,j}^h$  constituent the group  $i$ . For simplicity, we here assume that  $n^h$  does not depend of  
 193  $i$ , *i.e.* all groups of size belonging to the scale  $h+1$ , are constituted by the same number of  
 194 sample from the scale  $h$ . Then, for being representative of the importance of the variance of a  
 195 certain scale ( $h$ ) over the whole dataset one need to look at the mean of the scale variances of  
 196 the scale  $h$ , according to equation (6 and 7)

$$\overline{V^{h \rightarrow h+1}} = \frac{1}{N^{h+1}} \sum_{i=1}^{N^{h+1}} V_i^{h \rightarrow h+1} \quad (6)$$

w  
 ith

$$N^{h+1} = \prod_{p=h+1}^k n^p \quad (7)$$

197 Equation (7) describes that  $N^{h+1}$  is equal to the number of group whose size belonging to  
 198 the scale  $h+1$ . Thus, one can demonstrate (see Appendice 1) that for a dataset hierarchized  
 199 over  $k$  scale of interest, the variance (VAR) can be decomposed into the sum of the mean of  
 200 the scale variances (equation (8)):

$$VAR = V^{1 \rightarrow k} = \sum_{h=1}^{k-1} \overline{V^{h \rightarrow h+1}} \quad (8)$$

201

202 However, SVA requires a complete dataset with all values of scale 1 totally enumerated  
 203 (Moellering and Tobler, 1972). In our case, the data range over 8 orders of magnitude from  
 204 samples at the cm scale to a sampling area of hundreds of kilometres. Assuming 5 samples per  
 205 group, an exhaustive sampling would require  $5^7 = 78.125$  analyses. To overcome the  
 206 analytical limitation to produce so many analyses, a supplementary assumption is required:  
 207 the scale stability of relative variance. For each scale, this assumption assumes that all groups  
 208  $i$  are characterized by the same relative scale variance ( $RV^{h \rightarrow h+1}$ ). The  $RV^{h \rightarrow h+1}$  is defined as  
 209 the square of the relative standard deviation *i. e.* for any  $i$ :

$$RV^{h \rightarrow h+1} = \frac{V_i^{h \rightarrow h+1}}{(x_i^{h+1})^2} \quad (9)$$

210 This is a heavy assumption but it allows the calculation of any mean scale variance as soon  
 211 as both the relative scale variance and the sum of the square of the mean of all higher scale are  
 212 known (see Appendice 2) according to equation (10):

$$\text{For any } h \leq k-2 \quad \overline{V^{h \rightarrow h+1}} = \frac{RV^{h \rightarrow h+1}}{N^k} \prod_{i=h+1}^{k-1} (1 + RV^{i \rightarrow i+1}) \sum_{j=1}^{N^k} (x_j^k)^2 \quad (10)$$

213 This relation indicates that the means of the scale variances for a certain scale can be  
 214 calculated as soon as the relative scale variance is known. Lastly, this relation indicates that  
 215 direct comparison of the relative scale variance from different scales of the same dataset is not  
 216 meaningful and that comparison of the mean scale variance has to be preferred.

### 217 3.5.3 Experimental variogram

218 To complement Moran's Index, that compares samples to the global mean, and SVA, that  
 219 compares samples to a local mean, an experimental variogram was built. In this case, each  
 220 pair of samples is compared to the square of their difference without referring to any external  
 221 mean. Then, the gamma value ( $\gamma$ ) is computed as the half of the mean of the values that  
 222 belong to a certain distance, according to equation (11).

$$\gamma(d) = \sum_i^n \sum_{j \neq i}^n w_d(l_{ij}) (x_i - x_j)^2 \times \frac{1}{2 \sum_{i,j}^n w_d(l_{ij})} \quad (11)$$

$$w_d(l_{ij}) = \begin{cases} 1, & 10^d < l_{ij} < 10^{d+1} \\ 0, & \text{otherwise} \end{cases}$$

223

### 224 3.5.4 Application to the Loire estuary dataset

225 Moran's index, SVA and experimental variogram are calculated based on the average  
 226 density of *A. tepida* in the first centimetre depth measured in this study, in Thibault de

227 Chanvalon et al. (2015) and in the study of Mojtahid et al. (2016). This combined dataset is  
228 represented in Figure 1 and is not regularly distributed in the Loire area. For example, for the  
229 Moran's index calculation, each class of distance covering scales from centimetre to  
230 hectometre (hundreds of meters) are represented by less than 72 sample pairs. The scale  
231 variance analysis (SVA) was calculated based on regions delimited arbitrary by the black  
232 lines on the Figure 1. The column "available sampling / exhaustive sampling" in Table 1  
233 summarized the number of regions per scale and compared it with an exhaustive sampling as  
234 theoretically requested. The scale levels 3, 4 and 5 does not contain enough samples to be  
235 gathered into at least one group. Thus, the mean of the scale variance for scale 3, 4 and 5  
236 could not be calculated directly and was estimated by the difference between the global  
237 calculated variance and all the means of the scale variance. Moreover, all information for  
238 close ( $< 100$  m) samples belong to or are close to stations 1 and 2. Nevertheless, such  
239 limitations are very frequent in foraminiferal dataset and the spatial recovery obtained with  
240 this combined dataset is rare in the literature motivating the pursuit of the spatial  
241 heterogeneity analysis.

### 242 **3.6 Model of microhabitat equilibrium**

243 The relation between deep infaunal and shallow infaunal foraminiferal faunas is modelled  
244 using a dynamic 2 boxes-model (whose equations are detailed in Figure 2A) based on typical  
245 assumptions drawn from ecological studies (Levin, 1976). The shallow infaunal box is  
246 characterised by a population ( $pop_{sh}$ ), a first order mortality rate ( $k_{d_{sh}}$ ) and a reproduction rate  
247 described with the Verhulst equation, that is, a first order rate ( $k_p$ ) decreasing to zero as the  
248 population saturates ( $pop_{sat}$ ) available resources. The deep infaunal box is characterised by a  
249 population ( $pop_{de}$ ) and a first order mortality rate ( $k_{d_{de}}$ ). The transfer between the 2 boxes  
250 follows a first order rate ( $k_{ech}$ ), roughly estimating biomixing. The ratio of deep over shallow  
251 infaunal population,  $\alpha = pop_{de} / pop_{sh}$ , predicted by this model after an important increase of

252 environment capability (by 500 fold in this example) is shown in Figure 2B. First the shallow  
 253 population increase, hence  $\alpha$  decrease. After a short delay, deep infaunal population increase  
 254 too, leading to an equilibrium between exponentially growing shallow and deep infaunal  
 255 population and  $\alpha$  reaching a plateau ( $\alpha_{\text{exp}}$ , on Figure 2B). The higher  $k_{\text{ech}}$  is, the faster the first  
 256 plateau is reached. Finally, once the population reaches the limits of the environment  
 257 capabilities another equilibrium is observed between the two populations that is characterised  
 258 by a second plateau ( $\alpha_{\text{sat}}$  on Figure 2B). The higher  $k_p$  is, the faster the second plateau is  
 259 reached, other parameters having much less influence on the rate of  $\alpha$  changes. The  $\alpha$  value at  
 260 the plateau is defined as:

$$\alpha_{\text{sat}} = \frac{k_{\text{ech}}}{k_{\text{ech}} + k_{\text{d,de}}} \quad (1)$$

$$\alpha_{\text{exp}} = \begin{cases} 1 - \frac{b}{2} & \text{if } b \ll 2 \\ \frac{1}{b} & \text{if } b \gg 2 \end{cases}, \text{ with } b = \frac{k_p + k_{\text{d,de}} - k_{\text{d,sh}}}{k_{\text{ech}}} \quad (2)$$

261

262

263

## 4 Results

264

### 4.1 Environmental parameters

265

266

267

Table 2 summarizes most of the environmental parameters extracted from public survey databases (banque HYDRO, SYVEL and SHOM networks, see glossary) and previous publications (Benyoucef, 2014; Thibault de Chanvalon et al., 2016).

268

269

270

271

272

273

274

275

The two campaigns were characterized by contrasted river discharge ( $150 \text{ m}^3 \text{ s}^{-1}$  in September versus  $1200 \text{ m}^3 \text{ s}^{-1}$  in May), organic carbon content in the top of sediment (2.1 % versus 2.8 %), salinity (22 versus 8, respectively) and temperature ( $17 \text{ }^\circ\text{C}$  versus  $13 \text{ }^\circ\text{C}$ ). Contrastingly, nutrients showed mainly spatial variation with a higher concentration of dissolved phosphorus at Station 1, closer to the shore, with  $15.4$  and  $14.2 \text{ } \mu\text{mol L}^{-1}$  for September 2012 and May 2013 respectively, compared to  $2.7$  and  $4.8 \text{ } \mu\text{mol L}^{-1}$  for Station 2 (Thibault de Chanvalon et al., 2016). Finally, the oxygen penetration showed both important spatial and temporal variability with a lower value in May 2013.

276

### 4.2 Biological parameters

277

278

279

280

281

282

283

284

285

286

Table 3 indicates that the three studied biological compartments differ significantly between the two stations and less clearly between the two campaigns. Station 1 shows higher abundances of microphytobenthos (the average of the two campaign for chlorophyll A is  $340 \text{ mg m}^{-2}$  in Station 1 versus  $180 \text{ mg m}^{-2}$  in Station 2), macrofauna ( $770 \text{ ind m}^{-2}$  in Station 1 versus  $290 \text{ ind m}^{-2}$  in Station 2 on average) and living foraminifera ( $78 \text{ ind / } 10 \text{ cm}^3$  versus  $24 \text{ ind / } 10 \text{ cm}^3$ ) than Station 2. While *Ammonia tepida* (>70%) dominates foraminiferal communities in both stations, macrofaunal assemblages switch from a dominance of the polychaetes *Hediste diversicolor* (>75%) at Station 1 to a dominance of both the bivalve *Scrobicularia plana* and the polychaetes *Heteromastus filiformis* at Station 2. The main seasonal variation visible in both stations is for macrofauna with an increase of *H. filiformis*

287 associated to a decrease of *S. plana* in May 2013. However, in Station 1, but only there,  
288 foraminifer density decreases significantly in May 2013 with, for example, a near  
289 disappearance of *H. germanica* going from 36 ind / 10 cm<sup>3</sup> down to 2 ind / 10 cm<sup>3</sup> in the first  
290 top centimetre. The lability index (LI), that is higher than 0.9 in both stations and seasons,  
291 indicates important *in situ* autotrophic activity of microphytobenthos.

### 292 **4.3 Vertical distribution**

293 The densities of benthic foraminifera and Chl a concentration presented in Figure 3 show in  
294 several cases an exponential decrease of densities with depth. The high density of *H.*  
295 *germanica* in the top 2 millimetres in September 2012 at Station 1 (67 ind /10 cm<sup>3</sup>) appears  
296 concomitantly to particularly high densities of *A. tepida* (829 ind /10 cm<sup>3</sup>) and Chl a (201 mg  
297 m<sup>-2</sup>). However, in detail, the exponential decrease associated to this high density appears more  
298 progressive than for *A. tepida* and Chl a, with a minimum reached at 1.4 mm depth for *H.*  
299 *germanica* versus 0.6 mm depth for the others.

### 300 **4.4 Foraminifera aerobic respiration rates**

301 The respiration rates (RR) estimated for the foraminiferal population for each season and  
302 station as well as the relative foraminiferal contribution to DOU are shown in Table 4. The  
303 estimated respiration rates are  $3357 \pm 117$  pmol O<sub>2</sub>.ind<sup>-1</sup>.d<sup>-1</sup> and  $2154 \pm 75$  pmol O<sub>2</sub>.ind<sup>-1</sup>.d<sup>-1</sup>  
304 for *A. tepida* and  $685 \pm 134$  pmol O<sub>2</sub>.ind<sup>-1</sup>.d<sup>-1</sup> and  $439 \pm 86$  pmol O<sub>2</sub>.ind<sup>-1</sup>.d<sup>-1</sup> for *H. germanica*  
305 at respectively 17°C (September) and 13°C (May). The maximal relative contribution of the  
306 foraminiferal fauna to DOU was 2.3%, at station S1 in September 2012 mostly carried by the  
307 dense population of *A. tepida*. For all other samplings, foraminiferal respiration rates (sum of  
308 *A. tepida* and *H. germanica* respiration rates) are much lower and varies from 0.085 to 0.099  
309 mmol O<sub>2</sub> m<sup>-2</sup> d<sup>-1</sup>.

### 310 **4.5 Statistical analysis**

311 Figure 4A shows that the Moran's index is significantly higher than zero for all scales  
312 below 0.1 km, which indicates that foraminiferal densities are grouped into patches of  
313 hundreds of metre's size. The negative value for Moran's index between 1 and 10 km (Figure  
314 4A) indicates that most of the difference between environments occurs between 1 and 10 km  
315 for *A. tepida* densities. SVA results presented in Figure 4B (black dots) show that most of the  
316 variance (average scale variance > 10%) comes from the scales between 1 m and 1 km but the  
317 lack of data (see Table 1) prevents us from a better accuracy. Interestingly, scale variance  
318 analysis quantifies that scales between 1 cm and 1 m counting for 3.6 times less to the overall  
319 variance than the scales between 1 m and 1 km. Stability of SVA, even based on our sparse  
320 dataset, is illustrated by the white dots of Figure 4B. It shows that the SVA processed without  
321 the particularly dense Station 1 does not modify significantly the results. The Figure 4C  
322 shows the square differences of paired samples in grey dots. The variogram calculated for  
323 each distance range is particularly high between 100 m and 1 km.



324

## 5 Discussion

325

### 5.1 Critical scale of heterogeneity identified by multiscale analysis:

326

327

328

329

330

331

332

333

334

In “Les Brillantes” mudflat, our data show an overall high surface foraminiferal density (up to 829 ind. / 10 cm<sup>3</sup>) and very low diversity (only two different species identified) (Figure 3). High surface density (over 100 ind. / 10 cm<sup>3</sup>) of foraminiferal fauna is commonly reported in intertidal mudflat surfaces from estuaries (Debenay et al., 2006; Thibault de Chanvalon et al., 2015) or inlets (Alve and Murray, 1994; Cesbron et al., 2016; Goldstein et al., 1995) while a very low diversity is more typical of macrotidal estuaries. Indeed, only the species that are the most tolerant to large daily salinity variations can grow in macrotidal estuaries (Murray, 2006), especially on non-vegetated mud. These later are for instance known for their absence of agglutinated species (Berkeley et al., 2008).

335

336

337

338

339

340

341

342

343

344

345

346

347

Debenay and Guillou (2002) demonstrated that the estuarine compatible species colonize successive areas along the salinity gradient. However, they did not identify the preponderant forcing among all the parameters covarying with salinity. For example, in the Loire estuary, the regular dredging of the navigation channel has also been invoked to explain the extreme poverty of the diversity of the foraminifera fauna with only three living species reported over the whole salinity gradient (Mojtahid et al., 2016). In addition to the constrains specific to estuarine environments, more common forcing such as grain size, food availability or food quality would also modify foraminiferal growth opportunities and produce, *in fine*, an irregular surface density distribution such as that illustrated in Figure 1. In an attempt to catch such a variability, deterministic models (*e.g.* TROX model from Jorissen et al., 1995) build on predefined forcing, estimate compliance between a species and an environment while they hardly quantify the density variations. This issue is particularly critical in dynamic environments where kinetic effects, such as new colony settling (Alve, 1999; Weinmann and

348 Goldstein, 2017) may induce changes in hydrodynamic dispersal or hysteresis associated to  
349 transient environmental changes, prevail over saturation of the environment capabilities. A  
350 complementary approach used in ecological survey, based on geostatistical models (*e.g.*  
351 Talley, 2007) proposes at first, to synthetize spatial patterns in order to infer causality as a  
352 second step. From the three different geostatistical models chosen for this study (Moran's  
353 Index, SVA and experimental variogram, Figure 4) one common picture appears: most of the  
354 density variation comes from the scales between the metre scale, that gathers all paired  
355 samples distant from 1 to 10 m and the hectometre scale, that gathers all paired samples distant  
356 from 100 to 1000 m. The Moran's Index (Figure 4A) underlines particularly the hectometre  
357 scale where the Index decreases and crosses the zero line, changing from a distribution with  
358 almost similar densities (Moran Index above 0) to a distribution with contrasted or random  
359 densities (Moran Index value below or equal to zero, Figure 4A). The variogram plot (Figure  
360 4C) confirms the preponderant role of the hectometre scale with the highest gamma value  
361 calculated. Sadly, the lack of paired samples distant from 1 m to 100 m could hide unexpected  
362 changes and prevents us from being more precise about the most significant scale. Identical  
363 limitation is visible for the SVA that equally distributes the missing variance into the scales  
364 with missing paired samples (from metre to hectometre scale). However, SVA model predicts  
365 preponderant role of at least one of these scales by the difference between the overall variance  
366 to the variance attributed to the other scales. At all events, in order to maximize information  
367 on foraminiferal density spatial distribution, we recommend designing future sampling  
368 campaigns with stations distant from 1 metre to 1 kilometre, with a particular focus on the  
369 hectometre scale.

370 The geostatistical models are apparently in contradiction with the importance habitats  
371 succession along salinity gradient (Debenay and Guillou, 2002) since the SVA attributes only  
372 0.9 % of the total variance to the scale of salinity changes (over 100 km), the minimum

373 attributed to any scale. Qualitative analysis solves this discrepancy. For example, a qualitative  
374 SVA coded with values equal to 0 when no *Ammonia tepida* is observed, to 1 when *A. tepida*  
375 is a minor species (<10%) and equal to 2 when *A. tepida* is a major species (>10%) leads to  
376 drastically increase the importance of the estuarine scale (black diamonds on the Figure 4B).  
377 In the qualitative analysis, the scale over 10 km produces 41% of the total variance and  
378 therefore in strong agreement with the importance of the salinity gradient. Taken together,  
379 these results highlight the efficiency of deterministic models for qualitative predictions,  
380 understood as the order of magnitude of foraminiferal population densities and their lacks to  
381 quantify predictions. Geostatistical models represent promising tools to cross this gap  
382 especially when performed in combination with deterministic models. For example, scale  
383 analyses can be hyphenated with studies of environmental processes in order to associate one  
384 preponderant process to each scale of important variation. This exercise is proposed in the  
385 following discussion.

## 386        **5.2 Limiting factors at the Les Brillantes mudflat scale**

387        The focus on Les Brillantes mudflat allows investigation of processes explaining density  
388 variations over few hundreds of meters, a critical scale identified from the geostatistic models.  
389 On one hand, our results show that the two stations present very few qualitative differences,  
390 *i.e.* changes over order of magnitudes - the most significant being *H. germanica* in September  
391 2012 (Table 3) with high density in Station 1 probably produced by optimal conditions for  
392 development of propagules and/or reproduction during September weak riverine influence.  
393 This sensitivity tends to position *H. germanica* downstream from *A. tepida* in the estuarine  
394 succession as observed by Debenay et al., 2006 and Mojtahid et al., 2016 while Alve and  
395 Murray, 1994, Debenay et al., 2000 and Debenay and Guillou (2002) observations state for  
396 the opposite. On the second hand, quantitative differences between stations are observed on  
397 every variable with 1.5 to 5 fold more abundance of microphytobenthos, meiofauna and  
398 macrofauna at Station 1 (Table 3) and up to 5 fold faster respiration (Table 4). The longer  
399 emersion time, hence the longer light time exposure, and the higher nutrient input, probably  
400 streaming for the grazing land of the shore via a small channel (Table 2) might favour primary  
401 production compared to Station 2 and consequently may support higher density of fauna.

402        The exponential relation observed between Chl a and *A. tepida* (Figure 5A) indicates a  
403 possible deterministic relation between primary production and *A. tepida* at the hectometre  
404 scale and makes Chl a a good limiting factor for deterministic models at this scale. However,  
405 such a relation owes a lot to the opportunistic character of *A. tepida*, understood as the ability  
406 for a species to saturate rapidly the capabilities of an environment. Prolonging this  
407 interpretation, we can estimate that all parameters varying differently than Chl a have  
408 negligible effect on *A. tepida* density. Surprisingly, the co-varying parameters LI and the  
409 OPD, reputed to trace organic matter lability, evolved differently underlying the specific diet  
410 regime of *A. tepida*. Indeed, this species is known in the literature for being carnivorous

411 (Dupuy et al., 2010), predated on metazoan classes (Chronopoulou et al., 2019) and thus may  
412 ignore variation of primary production quality. Oppositely, the literature indicates that *H.*  
413 *germanica* feeds mostly on diatoms notably to steal their chloroplast (Pillet et al., 2011;  
414 Cesbron et al., 2017; Jauffrais et al., 2018; LeKieffre et al., 2018). It seems that this so-called  
415 “kleptoplasty” specialisation turns into a disadvantage when facing opportunistic species in  
416 low quality high quantity food environments.

417

### 418        **5.3 Vertical distribution of foraminifera: Microhabitat vs Bioturbation**

#### 419        **5.3.1 Biomixing and chemotaxis forcing**

420        The fine vertical sampling resolution (Figure 3) allows a precise description of the typical  
421 exponential vertical decrease of shallow infaunal microhabitat (Buzas et al., 1993). The very  
422 shallow density maximum indicates a favourable environment, supposedly a reproduction  
423 layer and/or propagule spawning event, due to high oxygen concentration and/or fresh organic  
424 matter (Berkeley et al., 2007; de Stigter et al., 1999; Geslin et al., 2004). The progressive  
425 decrease with depth is usually associated with the biomixing produced by macrofauna  
426 bioturbation (*e.g.* Alve and Bernhard, 1995; Saffert and Thomas, 1998; Thibault de  
427 Chanvalon et al., 2015), a predation-related strategy (De Stigter et al., 1998; Loubere, 1989)  
428 or the occurrence of oxygen oases around animal burrows (Goldstein et al., 1995; Steineck  
429 and Bergstein, 1979). However, the very steep decrease of *A. tepida* (minimum reached at 0.8  
430 cm depth) and the systematic slight re-increase at depth (except Station 2 in May 2013, Figure  
431 3) producing a shallow minimum density, corresponds to a specific pattern, likely produced  
432 by the combination of biomixing and chemotaxis (BC model, Thibault de Chanvalon et al.,  
433 2015). In this BC model, when buried close enough to the surface, the foraminifera detect the  
434 oxygenated layer and move back to the surface while, when buried deeper than their  
435 pseudopod length, the foraminifera are trapped at depth in a dormancy stasis, as observed by  
436 LeKieffre et al. (2017). The shallow minimum density corresponds to the chemotaxis range of  
437 the foraminifera. Oases model has been discarded in these stations because of the absence of  
438 correlation at the centimetre scale between deep living foraminifera and burrow traces  
439 (Thibault de Chanvalon et al., 2015).

440        In September 2012, when surface densities were high enough, *H. germanica* densities  
441 presented a similar pattern than *A. tepida* but with a less steep decrease since the shallow  
442 minimum is reached at 1.4 cm depth for *H. germanica* versus 0.6 mm for *A. tepida* (Figure 3).

443 On the line with the BC model, we interpret this observation as a wider chemotaxis range for  
444 *H. germanica*, maybe related to its pseudopod length, which feels necessary to move back to  
445 the surface once buried deeper than *A. tepida*. However, this difference could also come from  
446 *H. germanica* kleptoplasty, as proposed by Cesbron et al. (2017) in order to interpret similar  
447 observations. In this case, *H. germanica* would be less sensitive to oxygen depletion and  
448 tolerates being buried deeper before moving back to the surface.

### 449 5.3.2 Deep and shallow infaunal comparison

450 Based on the BC model, specimens' behaviour depends on their position compared to the  
451 shallow minimum, with upper specimens being more active and especially able to reproduce  
452 and growth while lower specimens are probably in dormancy stasis. When taking into account  
453 density results from the two sampling stations in September and in May, a linear positive  
454 correlation between these two populations appears (Figure 5B). It is a significant result as the  
455 line crosses the origin with a high  $R^2$  value (0.95) for *A. tepida*. The relation for *H. germanica*  
456 is less convincing since the lower observed population induces higher uncertainties. However,  
457 for *A. tepida*, this relevance is highlighted by other biological parameters measured in this  
458 study such as Chl a (Figure 5B) that does not follow any linear relation.

459 The model of microhabitat equilibrium (§3.6 and Figure 2) details explicitly, despite  
460 evident oversimplifications, how the shallow and deep infaunal population interaction can be  
461 describe by their ratio, so called  $\alpha$ , which depends of the intrinsic species dynamics  
462 (propagule spawning / reproduction and mortality rates), biomixing rate and the delay since  
463 the last change of available resources. After a certain point, function of biomixing and  
464 reproduction rate, the model shows that the time does not influence the  $\alpha$  value anymore, slow  
465 growing species being in exponential growth while faster growing species, such as  
466 opportunists, having already saturated the environment capabilities. The constancy of the  $\alpha$   
467 value found for *A. tepida* ( $\alpha = 1.1$ , Figure 5B) despite a 5 fold change of density indicates that

468 during each campaign, depth repartition of foraminifera population has reached an  
469 equilibrium since the last change of available resources, more likely a saturation equilibrium.  
470 Hence biomixing is fast relatively to foraminifera resource changes. This is not the case for  
471 Chl a probably because its main resource (available light) changes too fast compared to  
472 biomixing events while foraminifera populations average short term variations of food  
473 availability. Moreover, equation (11) indicates that an  $\alpha$  about 1 indicates high biomixing rate  
474 compared to mortality in anoxia, a first step to estimate biomixing rate using foraminifera  
475 vertical distribution. Taken together, analysis of vertical distribution confirms the steady state  
476 reached between surface resources and *A. tepida* density at surface and at depth and the  
477 importance of Chl a concentration at Les Brillantes. While the bioturbation intensity was  
478 expected to be a supplementary depth cause due to mortality increase at depth, this effect was  
479 not found to be significant since the highest density of foraminifera (including *H. germanica*)  
480 matches with the highest density of macrofauna (figure 5A).

## 481 **6 Conclusion**

482 Because of the several extreme conditions characterizing intertidal mudflat habitats,  
483 amongst which we can cite the risk of burial in anoxic sediments and the large daily salinity  
484 variation, the two species observed in “Les Brillantes” mudflat developed contrasting skills.  
485 *H. germanica* suffers from freshwater conditions during river flood periods but seems to get  
486 longer-range chemotaxis to face anoxia while *A. tepida* appears to be much less sensitive to  
487 freshwater inputs and favours dormancy as a strategy to overcome burial into anoxic depths.  
488 These differences could come from their different feeding strategies, *H. germanica* having a  
489 more specific diet while *A. tepida*, feeding from different sources, is emancipated from  
490 primary producer dependency and shows an opportunistic behaviour.



491 Geostatistic models confirm the effectiveness of average salinity to describe qualitatively  
492 the habitats distribution. However, they indicate that the density of foraminifera in these  
493 habitats are controlled by other parameters, such as Chl a, that varies over distance from 1 m  
494 and 1 km. These distances are often underrepresented in publications looking at foraminiferal  
495 heterogeneity and require supplementary investigations to state about their importance. Thus,  
496 we recommend to future models to fit geostatistical and deterministic approaches, for  
497 example, by associating a particular preponderant mechanism to each scale characterized by  
498 high heterogeneity.

## 499 **7 Acknowledgement**

500 This study is part of the RS2E–OSUNA project funded by the Région Pays de la Loire and  
501 benefits from the campaign Halioloire 1 (10.17600/12120050). The authors want to thank the  
502 associate editor and re-viewers for their valuable suggestions to improve this manuscript.  
503 Thanks also to E. Cheveau, E. Beneteau, A. Mouret, for their help during sampling and  
504 picking.

505

506

507

508

## 8 Glossary

509 SYVEL (Surveillance system of the Loire estuary) network maintains 6 high frequency  
510 stations between Nantes and Paimboeuf for physicochemical parameters of subsurface waters  
511 (temperature, salinity, dissolved oxygen concentration, and turbidity). Founded by the region  
512 Pays de la Loire.

513 SHOM is a french national military service for marine and coastal geographic information.

514 Banque HYDRO is a national public gathering hub of river flows, alimeted mainly by  
515 numerous national services.

516

## 9 Bibliography

517

518 Alve, E., 1999. Colonization of new habitats by benthic foraminifera: a review. *Earth-Sci.*  
519 *Rev.* 46, 167–185. [https://doi.org/10.1016/S0012-8252\(99\)00016-1](https://doi.org/10.1016/S0012-8252(99)00016-1)

520 Alve, E., Bernhard, J.M., 1995. Vertical migratory response of benthic foraminifera to  
521 controlled oxygen concentrations in an experimental mesocosm. *Mar Ecol Prog Ser* 116, 137–  
522 151. <http://dx.doi.org/10.3354/meps116137>

523 Alve, E., Murray, J.W., 2001. Temporal Variability in Vertical Distributions of Live  
524 (stained) Intertidal Foraminifera, Southern England. *J. Foraminifer. Res.* 31, 12–24.  
525 <https://doi.org/10.2113/0310012>

526 Alve, E., Murray, J. w, 1994. Ecology and taphonomy of benthic foraminifera in a  
527 temperate mesotidal inlet. *J. Foraminifer. Res.* 24, 18–27.  
528 <https://doi.org/10.2113/gsjfr.24.1.18>

529 Benyoucef, I., 2014. Télédétection visible proche-infrarouge de la distribution spatio-  
530 temporelle du microphytobenthos estuarien (Ph.D. thesis). Université de Nantes.

531 Berg, P., Risgaard-Petersen, N., Rysgaard, S., 1998. Interpretation of measured  
532 concentration profiles in sediment pore water. *Limnol. Oceanogr.* 43, 1500–1510.  
533 <https://doi.org/10.4319/lo.1998.43.7.1500>

534 Berkeley, A., Perry, C.T., Smithers, S.G., Horton, B.P., 2008. The spatial and vertical  
535 distribution of living (stained) benthic foraminifera from a tropical, intertidal environment,  
536 north Queensland, Australia. *Mar. Micropaleontol.* 69, 240–261.  
537 <https://doi.org/10.1016/j.marmicro.2008.08.002>

538 Berkeley, A., Perry, C.T., Smithers, S.G., Horton, B.P., Taylor, K.G., 2007. A review of the  
539 ecological and taphonomic controls on foraminiferal assemblage development in intertidal  
540 environments. *Earth-Sci. Rev.* 83, 205–230. <https://doi.org/10.1016/j.earscirev.2007.04.003>

541 Bianchi, T.S., Findlay, S., 1991. Decomposition of Hudson Estuary Macrophytes:  
542 Photosynthetic Pigment Transformations and Decay Constants. *Estuaries* 14, 65.  
543 <https://doi.org/10.2307/1351983>

544 Bird, C., Schweizer, M., Roberts, A., Austin, W.E.N., Knudsen, K.L., Evans, K.M.,  
545 Filipsson, H.L., Sayer, M.D.J., Geslin, E., Darling, K.F., 2020. The genetic diversity,  
546 morphology, biogeography, and taxonomic designations of *Ammonia* (Foraminifera) in the  
547 Northeast Atlantic. *Mar. Micropaleontol.* 155, 101726.  
548 <https://doi.org/10.1016/j.marmicro.2019.02.001>

549 Bivand, R.S., Wong, D.W.S., 2018. Comparing implementations of global and local  
550 indicators of spatial association. *TEST* 27, 716–748. [https://doi.org/10.1007/s11749-018-](https://doi.org/10.1007/s11749-018-0599-x)  
551 0599-x

552 Bradshaw, J.S., 1961. Laboratory experiments on the ecology of foraminifera. Cushman  
553 Found Foram Res Contr 12, 87–106.

554 Buzas, M.A., Culver, S.J., Jorissen, F.J., 1993. A statistical evaluation of the microhabitats  
555 of living (stained) infaunal benthic foraminifera. Mar. Micropaleontol. 20, 311–320.  
556 [https://doi.org/10.1016/0377-8398\(93\)90040-5](https://doi.org/10.1016/0377-8398(93)90040-5)

557 Cartaxana, P., Jesus, B., Brotas, V., 2003. Pheophorbide and pheophytin a-like pigments as  
558 useful markers for intertidal microphytobenthos grazing by *Hydrobia ulvae*. Estuar. Coast.  
559 Shelf Sci. 58, 293–297. [https://doi.org/10.1016/S0272-7714\(03\)00081-7](https://doi.org/10.1016/S0272-7714(03)00081-7)

560 Cesbron, F., Geslin, E., Kieffre, C.L., Jauffrais, T., Nardelli, M.P., Langlet, D., Mabilieu,  
561 G., Jorissen, F.J., Jézéquel, D., Metzger, E., 2017. Sequestered Chloroplasts in the Benthic  
562 Foraminifer *Haynesina Germanica*: Cellular Organization, Oxygen Fluxes and Potential  
563 Ecological Implications. J. Foraminifer. Res. 47, 268–278.  
564 <https://doi.org/10.2113/gsjfr.47.3.268>

565 Chronopoulou, P.-M., Salonen, I., Bird, C., Reichart, G.-J., Koho, K.A., 2019.  
566 Metabarcoding Insights Into the Trophic Behavior and Identity of Intertidal Benthic  
567 Foraminifera. Front. Microbiol. 10. <https://doi.org/10.3389/fmicb.2019.01169>

568 Coynel, A., Gorse, L., Curti, C., Schafer, J., Grosbois, C., Morelli, G., Ducassou, E., Blanc,  
569 G., Maillet, G.M., Mojtahid, M., 2016. Spatial distribution of trace elements in the surface  
570 sediments of a major European estuary (Loire Estuary, France): Source identification and  
571 evaluation of anthropogenic contribution. J. Sea Res. 118, 77–91.  
572 <https://doi.org/10.1016/j.seares.2016.08.005>

573 De Stigter, H., Jorissen, F., Van der Zwaan, G., 1998. Bathymetric distribution and  
574 microhabitat partitioning of live (Rose Bengal stained) benthic foraminifera along a shelf to  
575 bathyal transect in the southern Adriatic Sea. *J. Foraminifer. Res.* 28, 40–65.

576 de Stigter, H.C., van der Zwaan, G.J., Langone, L., 1999. Differential rates of benthic  
577 foraminiferal test production in surface and subsurface sediment habitats in the southern  
578 Adriatic Sea. *Palaeogeogr. Palaeoclimatol. Palaeoecol.* 149, 67–88.  
579 [https://doi.org/10.1016/S0031-0182\(98\)00193-X](https://doi.org/10.1016/S0031-0182(98)00193-X)

580 Debenay, J.-P., Guillou, J.-J., 2002. Ecological transitions indicated by foraminiferal  
581 assemblages in paralic environments. *Estuaries* 25, 1107–1120.  
582 <https://doi.org/10.1007/BF02692208>

583 Debenay, J.-P., Guillou, J.-J., Redois, F., Geslin, E., 2000. Distribution Trends of  
584 Foraminiferal Assemblages in Paralic Environments, in: Martin, R.E. (Ed.), *Environmental*  
585 *Micropaleontology*. Springer US, pp. 39–67.

586 Debenay, J.-P., Guillou, J.-J., Tsakiridis, E., de Casamajor, M.-N., 2001. Bioindicateurs  
587 d'impact dans les ports et les estuaires: les foraminifères. *Rev. Fr. Génie Civ.* 5, 1105–1122.

588 Dupuy, C., Rossignol, L., Geslin, E., Pascal, P.-Y., 2010. Predation of Mudflat Meio-  
589 Macrofaunal Metazoans by a Calcareous Foraminifer, *Ammonia tepida* (cushman, 1926). *J.*  
590 *Foraminifer. Res.* 40, 305–312. <https://doi.org/10.2113/gsjfr.40.4.305>

591 Fortin, M.-J., Dale, M.R.T., 2005. *Spatial analysis a guide for ecologists*. Cambridge  
592 University Press, Cambridge, N.Y.

593 Geslin, E., Heinz, P., Jorissen, F., Hemleben, Ch., 2004. Migratory responses of deep-sea  
594 benthic foraminifera to variable oxygen conditions: laboratory investigations. *Mar.*  
595 *Micropaleontol.* 53, 227–243. <https://doi.org/10.1016/j.marmicro.2004.05.010>

596 Goldstein, S.T., Watkins, G.T., Kuhn, R.M., 1995. Microhabitats of salt marsh  
597 foraminifera: St. Catherines Island, Georgia, USA. *Mar. Micropaleontol.*, Selected papers  
598 from the Fifth International Symposium of Foraminifera 26, 17–29.  
599 [https://doi.org/10.1016/0377-8398\(95\)00006-2](https://doi.org/10.1016/0377-8398(95)00006-2)

600 Hohenegger, J., Piller, W.E., Baal, C., 1993. Horizontal and vertical spatial  
601 microdistribution of foraminifers in the shallow subtidal Gulf of Trieste, northern Adriatic  
602 Sea. *J. Foraminifer. Res.* 23, 79–101. <https://doi.org/10.2113/gsjfr.23.2.79>

603 Jauffrais, T., LeKieffre, C., Koho, K.A., Tsuchiya, M., Schweizer, M., Bernhard, J.M.,  
604 Meibom, A., Geslin, E., 2018. Ultrastructure and distribution of kleptoplasts in benthic  
605 foraminifera from shallow-water (photic) habitats. *Mar. Micropaleontol.*, Benthic  
606 Foraminiferal Ultrastructure Studies 138, 46–62.  
607 <https://doi.org/10.1016/j.marmicro.2017.10.003>

608 Jorissen, F.J., de Stigter, H.C., Widmark, J.G.V., 1995. A conceptual model explaining  
609 benthic foraminiferal microhabitats. *Mar. Micropaleontol.* 26, 3–15.  
610 [https://doi.org/10.1016/0377-8398\(95\)00047-X](https://doi.org/10.1016/0377-8398(95)00047-X)

611 Kitazato, H., Shirayama, Y., Nakatsuka, T., Fujiwara, S., Shimanaga, M., Kato, Y., Okada,  
612 Y., Kanda, J., Yamaoka, A., Masuzawa, T., Suzuki, K., 2000. Seasonal phytodetritus  
613 deposition and responses of bathyal benthic foraminiferal populations in Sagami Bay, Japan:  
614 preliminary results from <sup>a</sup>Project Sagami 1996±1999<sup>o</sup>. *Mar. Micropaleontol.* 15.

615 Langlet, D., Baal, C., Geslin, E., Metzger, E., Zuschin, M., Riedel, B., Risgaard-Petersen,  
616 N., Stachowitsch, M., Jorissen, F.J., 2014. Foraminiferal species responses to in situ,  
617 experimentally induced anoxia in the Adriatic Sea. *Biogeosciences* 11, 1775–1797.  
618 <https://doi.org/10.5194/bg-11-1775-2014>

619 Legendre, P., Fortin, M.-J., 1989. Spatial pattern and ecological analysis. *Vegetation* 80,  
620 107–138.

621 LeKieffre, C., Jauffrais, T., Geslin, E., Jesus, B., Bernhard, J.M., Giovani, M.-E., Meibom,  
622 A., 2018. Inorganic carbon and nitrogen assimilation in cellular compartments of a benthic  
623 kleptoplastic foraminifer. *Sci. Rep.* 8, 1–12. <https://doi.org/10.1038/s41598-018-28455-1>

624 LeKieffre, C., Spangenberg, J.E., Mabilieu, G., Escrig, S., Meibom, A., Geslin, E., 2017.  
625 Surviving anoxia in marine sediments: The metabolic response of ubiquitous benthic  
626 foraminifera (*Ammonia tepida*). *PloS One* 12, e0177604.

627 Levin, S.A., 1976. Population Dynamic Models in Heterogeneous Environments. *Annu.*  
628 *Rev. Ecol. Syst.* 287–310.

629 Loubere, P., 1989. Bioturbation and sedimentation rate control of benthic microfossil taxon  
630 abundances in surface sediments: A theoretical approach to the analysis of species  
631 microhabitats. *Mar. Micropaleontol.* 14, 317–325. [https://doi.org/10.1016/0377-](https://doi.org/10.1016/0377-8398(89)90016-9)  
632 [8398\(89\)90016-9](https://doi.org/10.1016/0377-8398(89)90016-9)

633 Méléder, V., Barillé, L., Rincé, Y., Morançais, M., Rosa, P., Gaudin, P., 2005. Spatio-  
634 temporal changes in microphytobenthos structure analysed by pigment composition in a  
635 macrotidal flat (Bourgneuf Bay, France). *Mar. Ecol. Prog. Ser.* 297, 83–99.  
636 <https://doi.org/10.3354/meps297083>

637 Moellering, H., Tobler, W., 1972. Geographical Variances. *Geogr. Anal.* 4, 34–50.  
638 <https://doi.org/10.1111/j.1538-4632.1972.tb00455.x>

639 Mojtahid, M., Geslin, E., Coynel, A., Gorse, L., Vella, C., Davranche, A., Zozzolo, L.,  
640 Blanchet, L., Bénéteau, E., Maillet, G., 2016. Spatial distribution of living (Rose Bengal

641 stained) benthic foraminifera in the Loire estuary (western France). *J. Sea Res.*  
642 <https://doi.org/10.1016/j.seares.2016.02.003>

643 Murray, J.W., 2006. *Ecology and applications of benthic foraminifera*. Cambridge  
644 University Press, Cambridge.

645 Pillet, L., de Vargas, C., Pawlowski, J., 2011. Molecular Identification of Sequestered  
646 Diatom Chloroplasts and Kleptoplastidy in Foraminifera. *Protist* 162, 394–404.  
647 <https://doi.org/10.1016/j.protis.2010.10.001>

648 Richirt, J., Schweizer, M., Bouchet, V.M.P., Mouret, A., Quinchar, S., Jorissen, F.J., 2019.  
649 Morphological Distinction of Three *Ammonia* Phylotypes Occurring Along European Coasts.  
650 *J. Foraminifer. Res.* 49, 76–93. <https://doi.org/10.2113/gsjfr.49.1.76>

651 Saffert, H., Thomas, E., 1998. Living foraminifera and total populations in salt marsh peat  
652 cores: Kelsey Marsh (Clinton, CT) and the Great Marshes (Barnstable, MA). *Mar.*  
653 *Micropaleontol.* 33, 175–202. [https://doi.org/10.1016/S0377-8398\(97\)00035-2](https://doi.org/10.1016/S0377-8398(97)00035-2)

654 Schönfeld, J., Alve, E., Geslin, E., Jorissen, F., Korsun, S., Spezzaferri, S., 2012. The  
655 FOBIMO (FORaminiferal BIO-MONitoring) initiative—Towards a standardised protocol for  
656 soft-bottom benthic foraminiferal monitoring studies. *Mar. Micropaleontol.* 94–95, 1–13.  
657 <https://doi.org/10.1016/j.marmicro.2012.06.001>

658 Steineck, P.L., Bergstein, J., 1979. Foraminifera from Hommocks salt-marsh, Larchmont  
659 Harbor, New York. *J. Foraminifer. Res.* 9, 147–158.

660 Talley, T.S., 2007. Which spatial heterogeneity framework? Consequences for conclusions  
661 about patchy population distributions. *Ecology* 88, 1476–1489.



662 Thibault de Chanvalon, A., Metzger, E., Mouret, A., Cesbron, F., Knoery, J., Rozuel, E.,  
663 Launeau, P., Nardelli, M.P., Jorissen, F.J., Geslin, E., 2015. Two-dimensional distribution of  
664 living benthic foraminifera in anoxic sediment layers of an estuarine mudflat (Loire estuary,  
665 France). *Biogeosciences* 12, 6219–6234. <https://doi.org/10.5194/bg-12-6219-2015>

666 Thibault de Chanvalon, A., Mouret, A., Knoery, J., Geslin, E., Péron, O., Metzger, E.,  
667 2016. Manganese, iron and phosphorus cycling in an estuarine mudflat, Loire, France. *J. Sea*  
668 *Res.* 118, 92–102. <https://doi.org/10.1016/j.seares.2016.10.004>

669 Weinmann, A.E., Goldstein, S.T., 2017. Landward-directed Dispersal of Benthic  
670 Foraminiferal Propagules At Two Shallow-water Sites in the Doboy Sound Area (Georgia,  
671 U.S.A.). *J. Foraminifer. Res.* 47, 325–336. <https://doi.org/10.2113/gsjfr.47.4.325>

672 Wu, J., Jelinski, D.E., Luck, M., Tueller, P.T., 2000. Multiscale Analysis of Landscape  
673 Heterogeneity: Scale Variance and Pattern Metrics. *Geogr. Inf. Sci.* 6, 6–19.  
674 <https://doi.org/10.1080/10824000009480529>

675

676

## 10 Tables

677

**10.1 Table 1: Scale Variance Analysis**

Scale level (h)	Characteristic scale distances ( $10^{h-3}$ m)	Family size* ( $n^h$ )	Available sampling / exhaustive sampling	Relative scale variance ( $RV^{h \rightarrow h+1}$ )	$\frac{1}{N^h} \sum_{i=1}^{N^h} (x_i^h)^2$	Mean of the scale variance ( $\overline{V^{h \rightarrow h+1}}$ )	$\frac{\overline{V^{h \rightarrow h+1}}}{VAR} \times 100$	$\frac{\overline{V^{h \rightarrow h+1}}}{VAR} \times 100^\dagger$
8	100 km		1/1		5.904			
7	10 km	7	7/7	2.318		14.38	0.9	0.6
6	1 km	7	7/49	3.513		74.19	4.6	2.5
5	100 m	7	0/343				26.6	28.2
4	10 m	7	0/2 401				26.6	28.2
3	1 m	7	2/16 807				26.6	28.2
2	1 dm	5	106/84 035	0.083		114.85	7.1	4.6
1	1 cm	7	7/588 245	0.083		125.54	7.7	7.7

678

\*Number of samples of order h required to constitute a sample of order h+1, † calculated after exclusion of S1 from the dataset

679

680 **10.2 Table 2 : Geochemical parameters**

	Sept 2012	May 2013
Average flow (m <sup>3</sup> s <sup>-1</sup> )	150	1200
Salinity <sup>2</sup>	22 ± 5	8 ± 7
Water Temperature (°C) <sup>2</sup>	17 ± 0.5	13 ± 1
Tidal coefficient <sup>3</sup>	50 ± 10	80 ± 20
Grain size nomination <sup>4</sup> (0-5cm)	silty clay	silty clay
S1 Oxygen Penetration Depth (mm) (± SD)	2.3 (±0.4, n=12)	1.9 (±0.2, n=24)
Dissolved phosphorus in 0-1 cm <sup>5</sup> (μmol L <sup>-1</sup> )	15.4	14.2
Total Organic Carbone in 0-1 cm <sup>5</sup> (%)	2.3	2.8
Grain size nomination <sup>4</sup> (0-5cm)	silty clay	silty clay
S2 Oxygen Penetration Depth (mm) (± SD)	4.7 (±0.7, n=10)*	1.4 (±0.2, n=4)
Dissolved phosphorus in 0-1 cm <sup>5</sup> (μmol L <sup>-1</sup> )	2.7	4.8
Total Organic Carbone in 0-1 cm <sup>5</sup> (%)	2.1	2.8

681 \*Most of the profiles show bioturbation <sup>1</sup>measured at Mont-Jean sur Loire (banque  
682 HYDRO) <sup>2</sup>GIP Loire <sup>3</sup>SHOM, <sup>4</sup>from Benyoucef (2014) <sup>5</sup>from Thibault de Chanvalon et al.  
683 (2016)

684

## 10.3 Table 3: Biological parameters

		Sept 2012			May 2013		
		Mean	SD	n	Mean	SD	n
Microphytobenthos (mg m <sup>-2</sup> )	Chl a from 0 to 1 cm (mg.m <sup>-2</sup> )	384	121	3	295	185	3
	Lability Index from 0 to 1 cm	0.969	0.007	3	0.973	0.007	3
Marofaunal density (ind m <sup>-2</sup> )	<i>Hediste diversicolor</i>	635		1	631		1
	<i>Heteromastus filiformis</i>	16		1	25		1
	<i>Scrobicularia plana</i>	159		1	70		1
S1 Foraminiferal density (ind. / 10 cm <sup>-3</sup> )	<i>A. tepida</i> from 0 to 1 cm	245	3	2	123	21	2
	<i>A. tepida</i> from 1 to 5 cm	53	7	2	31	8	2
	<i>H. germanica</i> from 0 to 1 cm	36	2	2	2	1	2
	<i>H. germanica</i> from 1 to 5 cm	6		1	4	1	2
Foraminifera ALD <sub>5</sub> (cm)	<i>A. tepida</i>	1.54	0.17	2	1.74	0.03	2
	<i>H. germanica</i>	1.66		1	3.45	0.06	2
Microphytobenthos (mg m <sup>-2</sup> )	Chl a from 0 to 1 cm (mg.m <sup>-2</sup> )	166	25	3	198	22	3
	Lability Index from 0 to 1 cm	0.945	0.008	3	0.978	0.011	3
Marofaunal density (ind m <sup>-2</sup> )	<i>Hediste diversicolor</i>	25		1	51		1
	<i>Heteromastus filiformis</i>	83		1	159		1
	<i>Scrobicularia plana</i>	162		1	108		1
S2 Foraminiferal density (ind / 10 cm <sup>-3</sup> )	<i>A. tepida</i> from 0 to 1 cm	46	12	3	60	12	2
	<i>A. tepida</i> from 1 to 5 cm	11	1	3	10		1
	<i>H. germanica</i> from 0 to 1 cm	5	1	3	5	1	2
	<i>H. germanica</i> from 1 to 5 cm	4	1	3	5		1
Foraminifera ALD <sub>5</sub> (cm)	<i>A. tepida</i>	1.80	0.27	3	1.50		1
	<i>H. germanica</i>	2.76	0.21	3	2.67		1

## 10.4 Table 4: Respiration rate calculation

Sampling date	Station	Species	Total number of foraminifera in the oxic zone (ind. 50cm <sup>-2</sup> )			DOU (mmolO <sub>2</sub> m <sup>-2</sup> d <sup>-1</sup> )			RR by foraminiferal population (mmolO <sub>2</sub> m <sup>-2</sup> d <sup>-1</sup> )			Foraminiferal contribution to DOU %	
			Mean	SD	n	mean	SD	n	mean	SD	n	mean	SD
September 2012	S1	<i>Ammonia tepida</i>	1053	77	2	24	10.9	12	0.557	0.152	2	2.3	0.6
		<i>H. germanica</i>	108	28	2	24	10.9	12	0.009	0.005	2	0	0
	S2	<i>Ammonia tepida</i>	144	38	3	9.1	4.5	10	0.097	0.025	3	1.1	0.3
		<i>H. germanica</i>	12	4	3	9.1	4.5	10	0.002	0	3	0	0
May 2013	S1	<i>Ammonia tepida</i>	217	1	2	71	31	7	0.093	0	2	0.1	0
		<i>H. germanica</i>	2	1	2	71	31	7	0	0	2	0	0
	S2	<i>Ammonia tepida</i>	198	36	3	56	15	3	0.085	0.015	3	0.2	0
		<i>H. germanica</i>	2	1	3	56	15	3	0	0	3	0	0

688

## 11 Figures

689

11.1 Figure 1: Bathymetry of the Loire estuary with surface density of *A. tepida* from Mojtahid et al. (2016) sampled in September

690

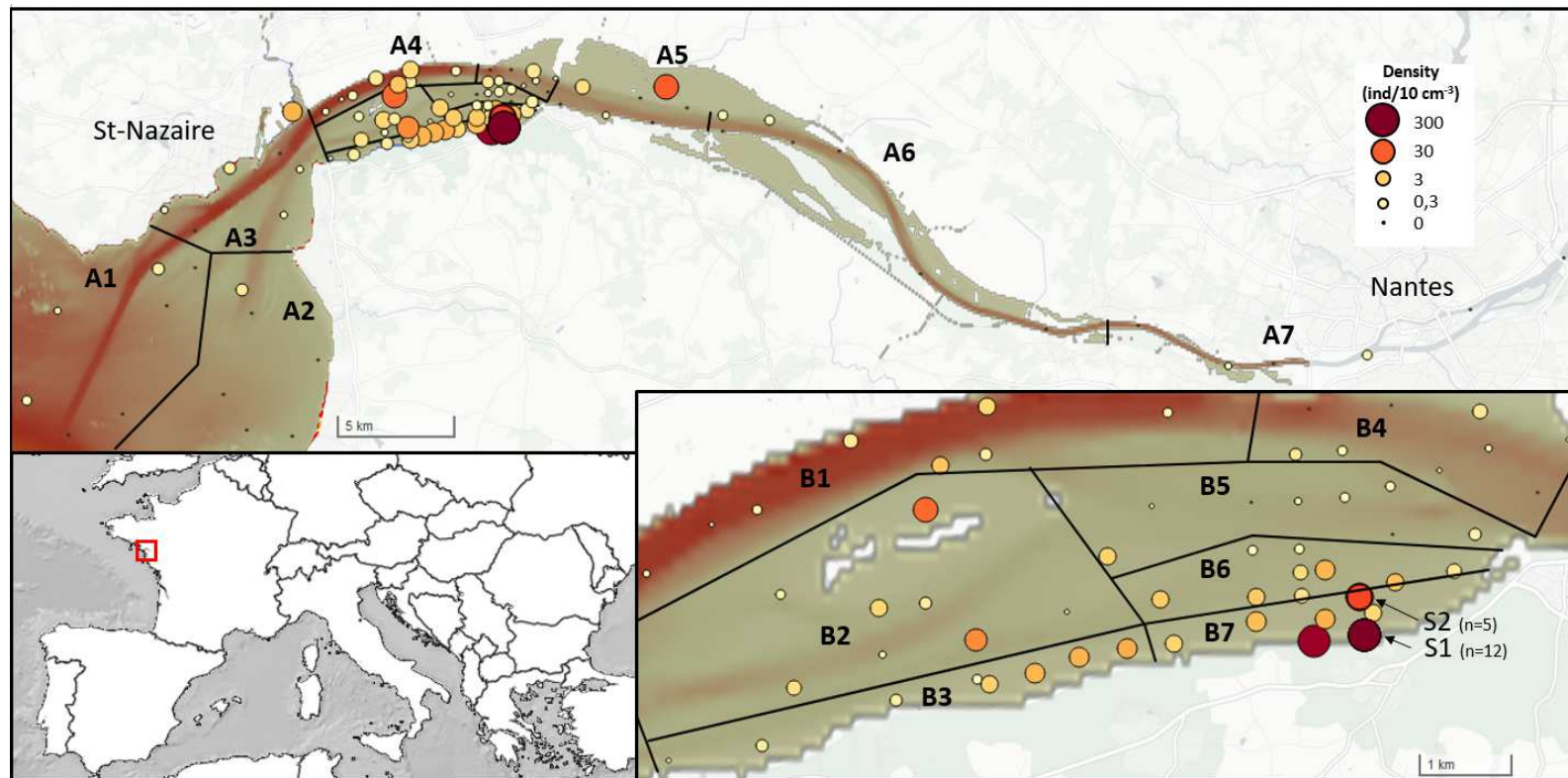
2012, Thibault de Chanvalon et al. (2015) sampled in May 2013 and this study (both May 2013 and September 2012). Black lines

691

indicate regions used in the scale variance analysis for the scale 7 (A1 to A7) and the scale 6 (B1 to B7). Bottom right insert focus

692

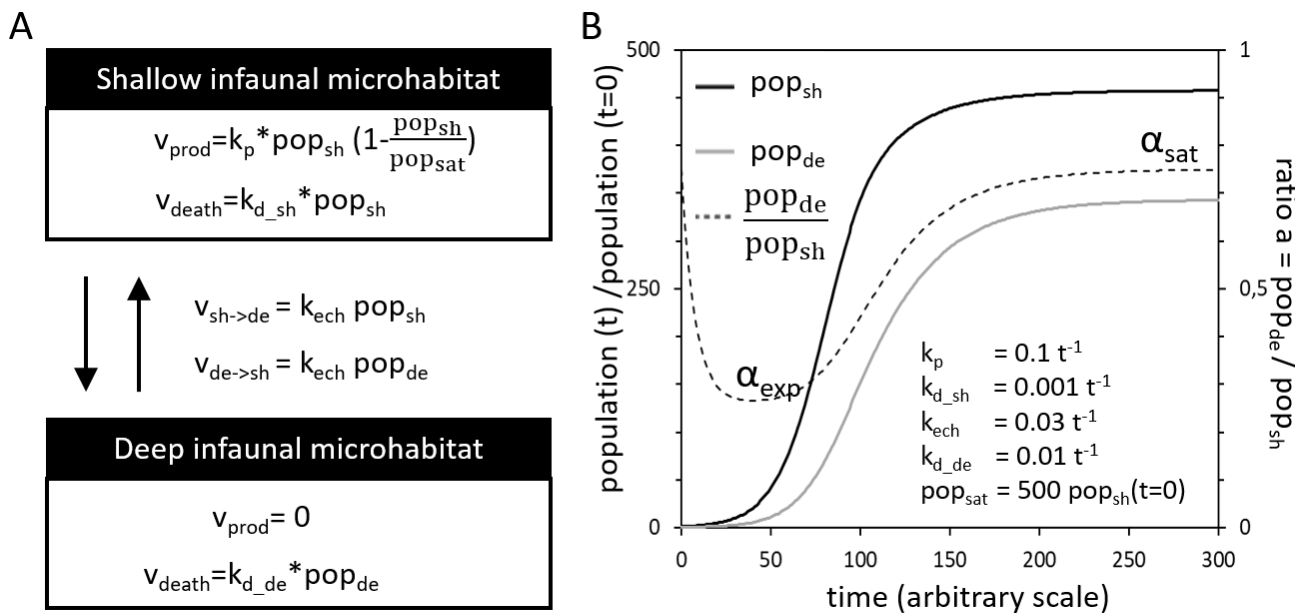
on the “Les Brillantes” mudflat (Map produced on R using leaflet package, bathymetry from the SHOM).



693

694 **11.2 Figure 2: A. Deterministic model to explain these relations based on biomixing**  
 695 **and chemotaxis forcing.**

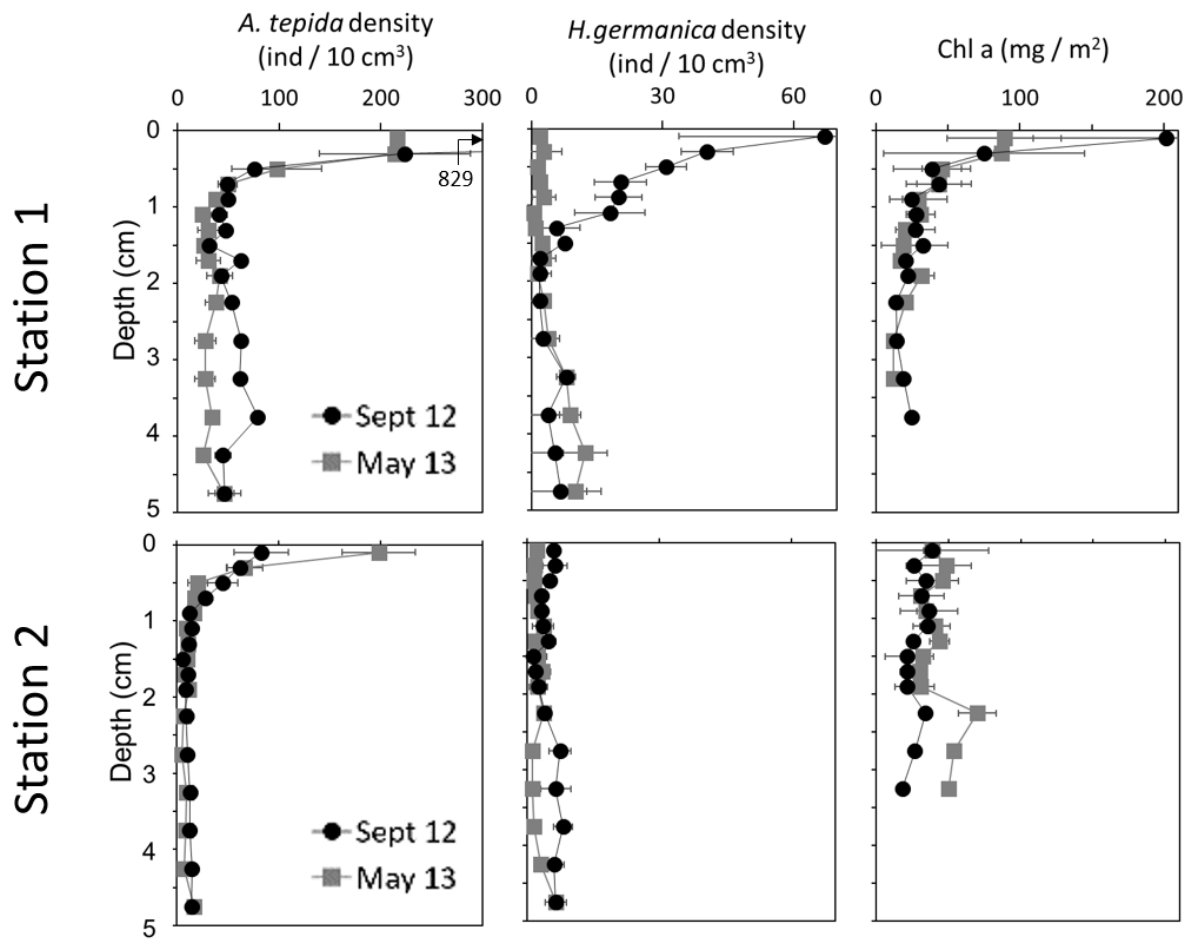
696  $v_{\text{prod}}$ ,  $v_{\text{death}}$ ,  $v_{\text{sh} \rightarrow \text{de}}$  and  $v_{\text{de} \rightarrow \text{sh}}$  correspond to the rate of reproduction, the rate of death, the  
 697 rate of exchange from shallow to deep microhabitat and the rate of exchange from deep to  
 698 shallow microhabitat respectively.  $k_p$ ,  $k_{d\_sh}$ ,  $k_{d\_de}$  and  $k_{\text{ech}}$  are the associated parameters while  
 699  $\text{pop}_{\text{sh}}$  and  $\text{pop}_{\text{de}}$  are the population of shallow and deep microhabitat. B. Example of a  
 700 representative result from the model following a 500 fold increase of environment capability ,  
 701 *i. e.* 500 fold  $\text{pop}_{\text{sat}}$  increase.



702

703

704 **11.3 Figure 3: Vertical distribution in the sediment column of living benthic**  
705 **foraminifera and Chlorophyll a.**



706

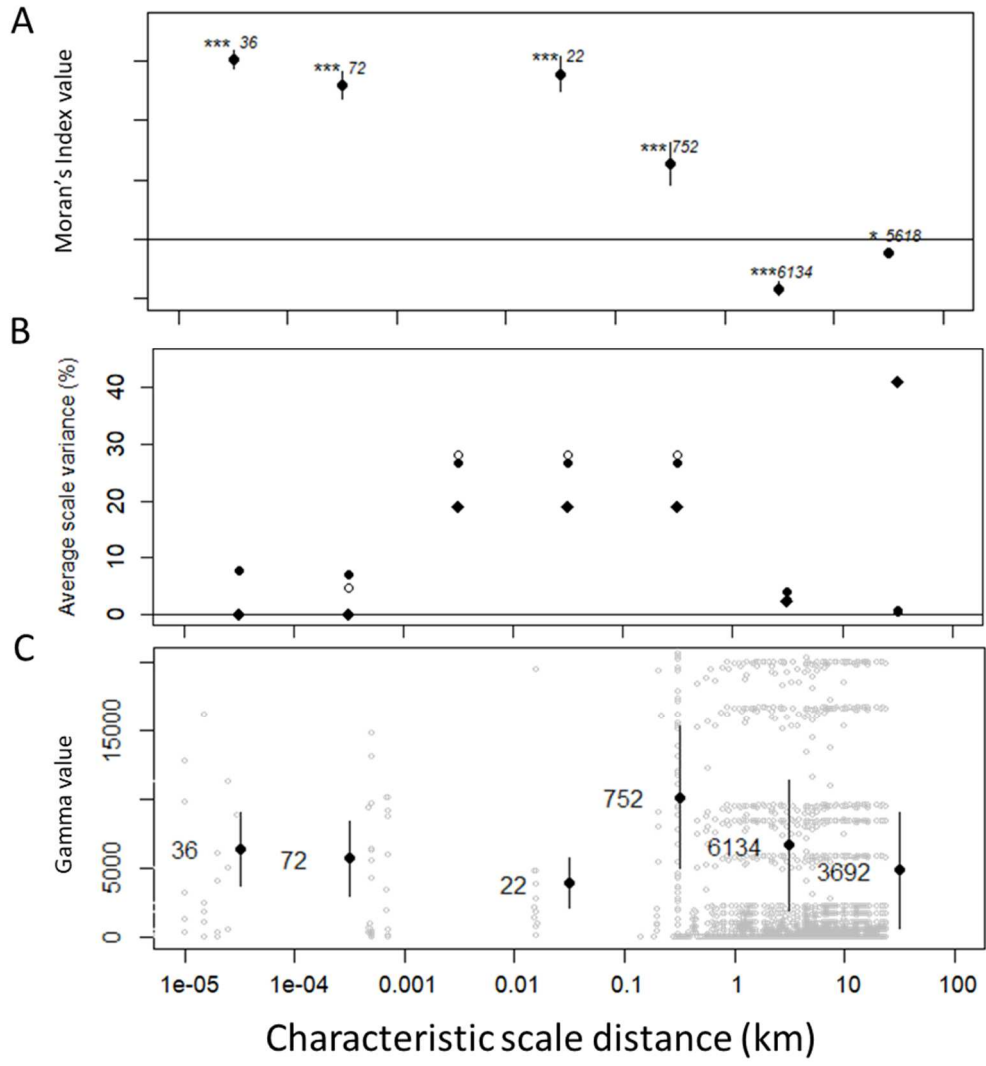
707

708



709 **11.4 Figure 4: Geostatistical model processes with the dataset from Figure 1 (black**  
710 **dots).**

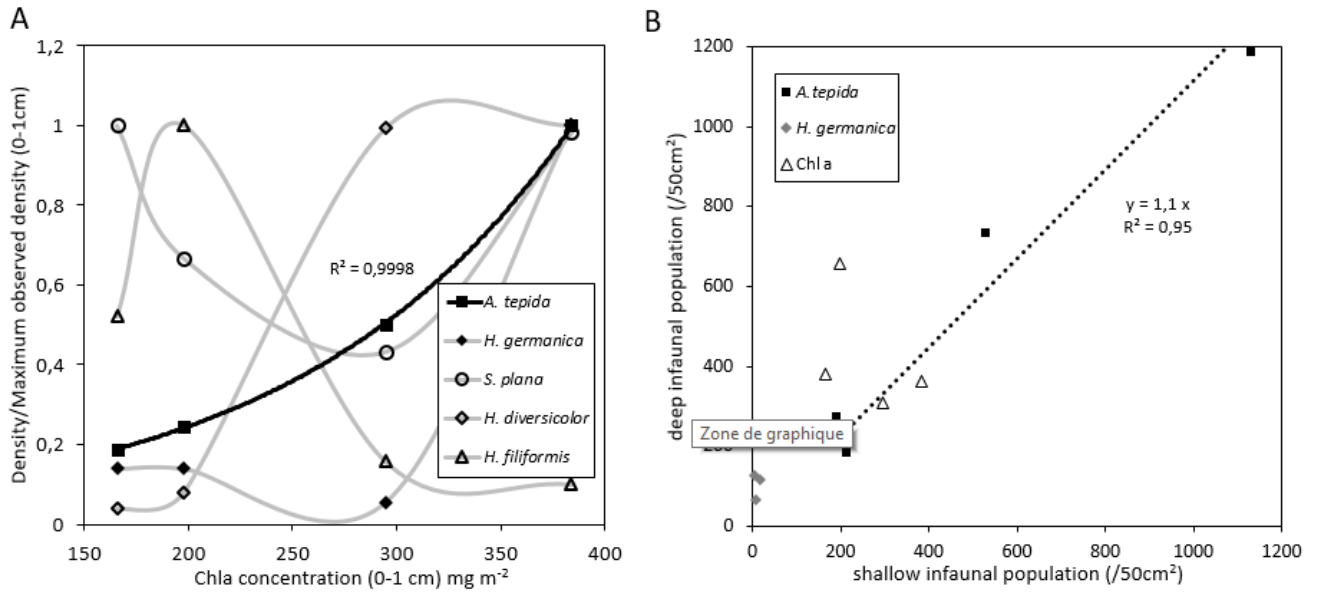
711 Error bars in Figure A corresponds to twice the standard deviation of the distribution  
712 obtained when the samples are randomly distributed (number of simulation is 104; star  
713 attribution is based on p-value;  $\leq 0.01^{***}$ ;  $\leq 0.05^{**}$ ;  $\leq 0.1^*$ ). In Figure B open circle  
714 represents the scale variance analysis (SVA) after exclusion of S1 from the dataset (open  
715 circle) and using qualitatively transformed dataset (black diamonds, see text for details). In  
716 the experimental variogram (Figure C), grey dots correspond to the square of the difference of  
717 each possible pairs, plotted against their distance. The black dots correspond to the mean and  
718 the error bars to a third of the standard deviation for each scale of distance between samples.



719

720

721 **11.5 Figure 5: A. Evolution of biological parameters in Les Brillantes according to**  
 722 **Chl a (data from Table 2). B. Relation between deep infaunal and shallow**  
 723 **infaunal population of *A. tepida* and *H. germanica* in Les Brillantes.**



724

725

726

## 12 Appendices

727

### 12.1 Appendix 1: Demonstration that the variance of a dataset hierarchized over k

728

scale is equal to the sum of the mean scale variance of each scale.

729

Based on the definition of the variance and on the formalism previously described,

730

samples' value are the  $x_i^1$  (they belong to the scale 1) and the global mean is  $x^k$ , we have :

$$VAR = V^{1 \rightarrow k} = \frac{1}{N^1} \sum_{i=1}^{N^1} (x_i^1 - x^k)^2 \quad \text{A}$$

1

$$V^{1 \rightarrow k} = \frac{1}{N^1} \left( \sum_{i=1}^{N^1} (x_i^1)^2 - N^1 (x^k)^2 \right) \quad \text{A}$$

2

731

The samples can be gathered in  $n^{k-1}$  group whose extension belong to the scale k-1. There is

732

$N^1 / n^{k-1}$  samples per group and the  $x_j^{k-1}$  are the means of each groups and the  $x_i^1$  are now

733

written as  $x_{i,j}^1$ , with the subscript j indicates to which groups the sample belong.

$$V^{1 \rightarrow k} = \frac{1}{N^1} \left( \sum_{i=1}^{N^1} (x_{i,j}^1)^2 - \sum_{j=1}^{n^{k-1}} \frac{N^1}{n^{k-1}} (x_j^{k-1})^2 + \sum_{j=1}^{n^{k-1}} \frac{N^1}{n^{k-1}} (x_j^{k-1})^2 - N^1 (x^k)^2 \right)$$

$$V^{1 \rightarrow k} = \frac{1}{N^1} \sum_{j=1}^{n^{k-1}} \left( \sum_{i=1}^{\frac{N^1}{n^{k-1}}} (x_{i,j}^1)^2 - \frac{N^1}{n^{k-1}} (x_j^{k-1})^2 \right) + \frac{1}{n^{k-1}} \left( \sum_{j=1}^{n^{k-1}} (x_j^{k-1})^2 - n^{k-1} (x^k)^2 \right)$$

$$V^{1 \rightarrow k} = \frac{1}{N^1} \sum_{j=1}^{n^{k-1}} \frac{N^1}{n^{k-1}} V_j^{1 \rightarrow k-1} + V^{k-1 \rightarrow k}$$

$$V^{1 \rightarrow k} = \frac{1}{n^{k-1}} \sum_{j=1}^{n^{k-1}} V_j^{1 \rightarrow k-1} + V^{k-1 \rightarrow k} \quad \text{A3}$$

734

The property expressed by A3 is true also for any j and p,  $V_j^{1 \rightarrow k-p}$ , especially

$$V_j^{1 \rightarrow k-1} = \frac{1}{n^{k-2}} \sum_{l=1}^{n^{k-2}} V_{j,l}^{1 \rightarrow k-2} + V_j^{k-2 \rightarrow k-1} \quad \text{A4}$$

735

Once you inject A4 into A3 you get,

$$V^{1 \rightarrow k} = \frac{1}{n^{k-1}} \frac{1}{n^{k-2}} \sum_{j=1}^{n^{k-1}} \sum_{l=1}^{n^{k-2}} V_{j,l}^{1 \rightarrow k-2} + \frac{1}{n^{k-1}} \sum_{j=1}^{n^{k-1}} V_j^{k-2 \rightarrow k-1} + V^{k-1 \rightarrow k} \quad \text{A51}$$

736 Then using the property expressed by A3 for p=2 you get

$$V^{1 \rightarrow k} = \frac{1}{n^{k-1}} \frac{1}{n^{k-2}} \frac{1}{n^{k-3}} \sum_{j=1}^{n^{k-1}} \sum_{l=1}^{n^{k-2}} \sum_{m=1}^{n^{k-3}} V_{j,l,m}^{1 \rightarrow k-3} + \frac{1}{n^{k-1}} \frac{1}{n^{k-2}} \sum_{j=1}^{n^{k-1}} \sum_{l=1}^{n^{k-2}} V_{j,l}^{k-3 \rightarrow k-2} + \frac{1}{n^{k-1}} \sum_{j=1}^{n^{k-1}} V_j^{k-2 \rightarrow k-1} + V^{k-1 \rightarrow k} \quad \text{A61}$$

737 Repeating this for all p until p=k-2

$$V^{1 \rightarrow k} = \frac{1}{N^2} \sum_{j=1}^{n^{k-1}} V_j^{1 \rightarrow 2} + \dots + \frac{1}{N^{k-2}} \sum_{j=1}^{N^{k-2}} V_j^{k-3 \rightarrow k-2} + \frac{1}{N^{k-1}} \sum_{j=1}^{N^{k-1}} V_j^{k-2 \rightarrow k-1} + V^{k-1 \rightarrow k} \quad \text{A71}$$

$$VAR = V^{1 \rightarrow k} = \sum_{h=1}^{k-1} \frac{1}{V^{h \rightarrow h+1}}$$

738

739 **12.2 Appendix 2: Demonstration of the expression of the mean of the scale variance**  
 740 **as a function of the relative scale variance**

741 Based on the relative scale variance definition, for any i :

$$RV^{h \rightarrow h+1} = \frac{1}{(x^{h+1})^2} \left( \frac{1}{n^h} \sum_{i=1}^{n^h} (x_i^h)^2 - (x^{h+1})^2 \right) \quad \text{B1}$$

742 Once reorganized, we get:

$$\sum_{i=1}^{n^h} (x_i^h)^2 = (1 + RV^{h \rightarrow h+1}) n^h (x^{h+1})^2$$

743 By sum over all the j group from the scale h+1,

$$\sum_{j=1}^{N^{h+1}} \sum_{i=1}^{n^h} (x_i^h)^2 = \sum_{j=1}^{N^{h+1}} (1 + RV^{h \rightarrow h+1}) n^h (x^{h+1})^2$$

$$\sum_{i=1}^{N^h} (x_i^h)^2 = (1 + RV^{h \rightarrow h+1}) n^h \sum_{j=1}^{N^{h+1}} (x_j^{h+1})^2 \quad \text{B2}$$

744 The equation B2 express the sum of the square at the scale h, as a function of the sum of the  
 745 square at the scale h+1. Injecting p times the equation B2 into itself, we get:

$$\sum_{i=1}^{N^h} (x_i^h)^2 = \prod_{i=h}^{h+p-1} (1 + RV^{i \rightarrow i+1}) n^i \sum_{j=1}^{N^{h+p}} (x_j^{h+p})^2 \quad \text{B3}$$

746 On another hand, taking the definition of the mean scale variance, we have:

$$\overline{V^{h \rightarrow h+1}} = \frac{1}{N^{h+1}} \sum_{i=1}^{N^{h+1}} (x_i^{h+1})^2 RV^{h \rightarrow h+1} \quad \text{B4}$$

747 Injecting B3 into B4, with p=k-1-h,

$$\begin{aligned} \overline{V^{h \rightarrow h+1}} &= \frac{RV^{h \rightarrow h+1}}{N^{h+1}} \prod_{i=h+1}^{k-1} (1 + RV^{i \rightarrow i+1}) n^i \sum_{j=1}^{N^k} (x_j^k)^2 \\ \overline{V^{h \rightarrow h+1}} &= \frac{RV^{h \rightarrow h+1}}{N^k} \prod_{i=h+1}^{k-1} (1 + RV^{i \rightarrow i+1}) \sum_{j=1}^{N^k} (x_j^k)^2 \end{aligned} \quad \text{B5}$$

748

749

750